Torque and Ripple Analyses of a Small BLDC Motor for a Surgical Device

Cheol Kim and Mingzhe Li
Department of Mechanical Engineering, Kyungpook National University, Daegu, South Korea
Email: kimchul@knu.ac.kr; limingzhe19880708@live.cn

***Abstract*— A small brushless direct current (BLDC) motor is under consideration to operate small dental and surgical hand-pieces instead of low-torque air turbines because of its high torque density. Electromagnetic analyses were carried out numerically to improve the performance of a hand-piece motor such as torque output and torque ripple. Several case studies on the characteristics of electromagnetic torque outputs were carried out by increasing the number of wound coil wires from 11 to 30, and the maximum motor torque was obtained using 20 wound wires at an electromagnetic angle of 90 °. The stator slot made of Teflon was found to be better than that made of steel in terms of magnetic flux density based from a material comparison study. In an effort to reduce the torque ripple of the motor, the changes in torque ripples for several slot shapes of a stator were evaluated by finite element analyses and compared. The slot with both circular holes and V-cut showed the best ripple performance of 6.10%, compared to 7.80% of the current design.**

***Index Terms*—BLDC motor, motor torque, medical hand-piece, stator coil, ripple, finite element method**

I. Introduction

Small hand-pieces have been widely used to cure diseased teeth and tissues in various dental and surgical operations [1]-[3]. Most dental hand-pieces have used an air turbine as a driving engine for the last 30 years [4]-[9]. The hand-piece driven by an air turbine, however, has difficulty in obtaining enough output torque and sometimes stops to rotate because of contamination of burrs. Recently, research is underway to replace the air turbine with a series of a gear train with an electric motor. The brushless direct current (BLDC) motor is widely used in various industries because it has a long life, low noise, higher speed, and higher torque and can be easily made smaller. The new hand-piece under development consists of a small driving BLDC motor, a small high-speed gear train, and a small burr. The mating gears usually rotate at 50,000–200,000 rpm to transfer power to the end of a burr by way of a series of high-speed gear train. Because BLDC motors have several advantages over general brushed DC or induction motors, including more torque per weight, more torque per watt, increased reliability, reduced noise, longer lifetime (no brush and commutator erosion), elimination of ionizing sparks from the commutator, and overall reduction of electromagnetic interference, its applications are very broad in various industries [10]-[12].

Structural optimization was performed for magnetic devices in a magnetic field using a homogenization method [13]-[15]. A new configuration of a brushless DC motor without a permanent magnet was studied using finite element analysis [16]. A design method of a single-phase brushless DC fan motor was studied to obtain optimal driving efficiency [17]. In addition, research on the reduction of torque ripple was performed for a synchronous reluctance motor using an asymmetric flux barrier arrangement [18]. The Taguchi optimization method was used in an effort to reduce torque ripple in interior permanent magnet motors [19]. The shape design of a hole in a motor rotor was prepared by drilling axial circular holes of optimal radius and position in the flux path of the rotor core. The torque curves of the optimized motor showed lower pulsating torque and higher average torque [20]. Structural optimization based on the level-set method was formulated to reduce torque ripples by minimizing the difference between torque values at defined rotor positions and the constant target average torque value under the constrained material usage [21]. A new optimization technique was applied to design the rotor of an interior permanent magnet motor which consists of a permanent magnet and ferromagnetic material for reducing the torque ripple. To express three different material properties (PM, FM, and air), a multi-phase level-set model representing two level-set functions was introduced, and the concept of a phase-field model was incorporated to distribute level-set functions for controlling the complexity of the structural boundaries [22]. The genetic algorithm was applied to minimize the torque ripple of a BLDC motor [23]. Several design modifications of the magnet were suggested to reduce the torque ripple [24]-[26].

There are few studies on the performance analyses of high-speed small BLDC motors particularly used for various medical hand-pieces for many types of medical operations. In this study, electromagnetic analyses were performed using MAXWELL program to improve the torque outputs of the hand-piece BLDC motor. The electromagnetic numerical results were compared with the measured ones. Variations in motor torque were calculated according to changes in the number of winding coils, and then, the number of coils that can increase torque outputs was determined. In addition, the study on

Manuscript received August 31, 2017; revised November 16, 2017.

doi: 10.18178/ijeetc.7.1.15-20

torque ripple was also conducted to obtain a good slot shape of a stator which could give lower torque ripple. Torque ripple refers to a periodic increase or decrease in output torque as the output shaft rotates. It is measured as the difference in maximum and minimum torque values over one complete revolution, generally expressed as a percentage.

II. Motor Torque Analysis

A. Electromagnetic Modeling

Fig. 1 shows a surgical hand-piece and a BLDC motor assembly that is composed of a sensor, a rotor, and a stator. The reference BLDC motor (which is an existing design) for this study has a diameter of 20 mm and a length of 30.0 mm. The sensor controls the flow of electric current by sensing the sequence, position, and speed of the rotor. The rotor consists of a rotating shaft and an Nd–Fe–B permanent magnet with S and N poles, and the stator is composed of coils, slots, and a cover. As electric current run through the coil, an electromagnetic force is generated. The coils, slots, and cover are made of brass, Teflon, and steel, respectively. The locations of the key parts in the stator and the rotor are described in Fig. 2.

(a) An example of a surgical hand-piece

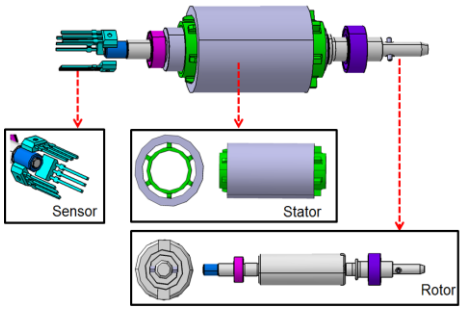

(b) Motor parts

Figure 1. A BLDC motor assembly and its parts used for a small surgical hand-piece.

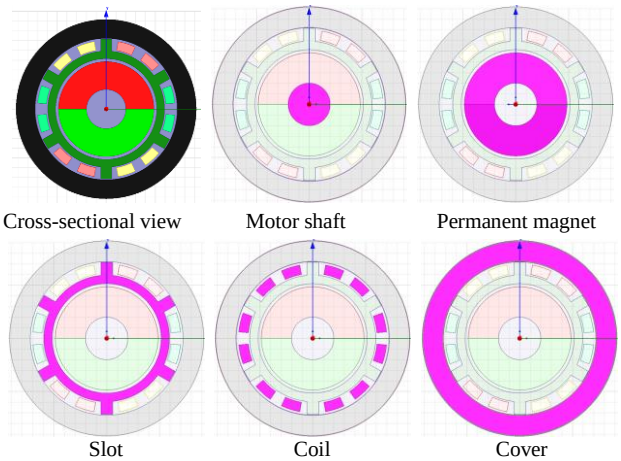

Figure 2. Locations of the key parts in the cross-section of the reference stator and rotor.

In Fig. 3, three bunches of coils denoted as 1, 2, and 3 that are located in a pair with an angle of 180 °in opposite directions and a permanent magnet in the central region are represented. As the rotor spins, the current in the stator coils varies, and the direction of the electromagnetic field also changes. Because a three-phase current is applied to operate the motor, current flows only through two coils, with no current in the rest of the coils. Fig. 4 shows how two directions of electromagnetic forces vary as the electric current path shifts from coil to coil wound at the stator and the magnet rotor at the center rotates in 1/4 cycle. The direction of the electromagnetic forces produced by the magnet is denoted by a dotted arrow and coils by a solid arrow, respectively, where "x" denotes current going in and "●" denotes current going out.

The direction of the electromagnetic force produced by the central magnet is denoted as a dotted arrow and that by stator coils is represented by a solid arrow. The marks "x" and "●" at slots denote current going in and out, respectively. Figs. 4(a), (b), (c), and (d) show the angles between two electromagnetic forces, i.e., 90 °, 120 °, 60 °, and 90 °, respectively.

The angle between the magnetic field directions of a rotor and a stator always exists between 60 ° and 120 °. The largest motor torque occurs at 90 °, and the smallest torque occurs at 60 ° or 120 °. The largest and smallest torque values were calculated using MAXWELL 2-D.

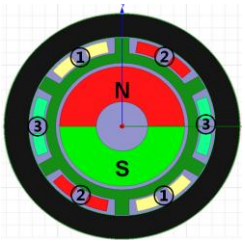

Figure 3. Three coils (1, 2, and 3) and a permanent magnet in the cross-section of a BLDC motor.

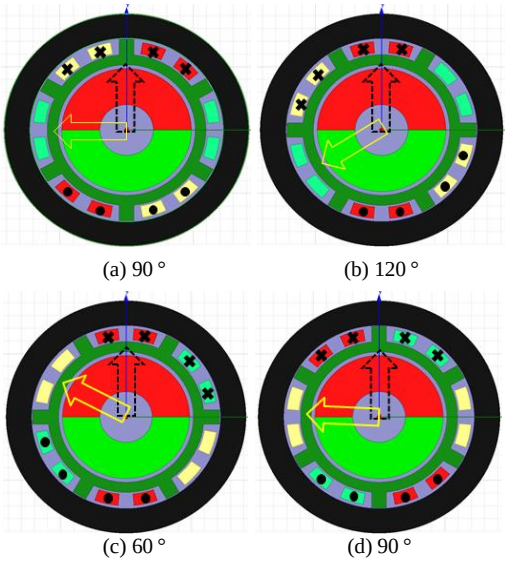

(a) 90 ° (b) 120 °

(c) 60 ° (d) 90 °

Figure 4. Directions of the electromagnetic forces produced by the magnet (dotted arrow) and coils (solid arrow), where "x" denotes current going in and "●" denotes current going out.

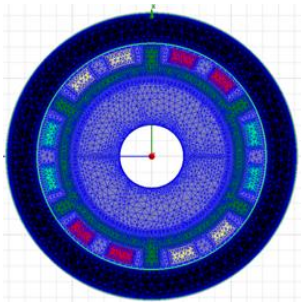

Figure 5. FE model of a BLDC motor.

Fig. 5 shows a finite element model of a BLDC motor constructed using three-noded elements. The vector potential at the outer circumference of the motor cross-section was set to be zero. The coercive force of the magnet is 10,500 Oe (Oersted), and the remanence is 14,000 Gauss. The rotor and the cover are made of SUS303F, whose magnet permeability is 1.008. As a current of 2.5 A runs through the coil and 12 coils are wound around a slot, the total current is 30 A. The slot is made of Teflon material, whose relative permeability is 1.0.

B. Electromagnetic Analysis

The magnetic flux density is the largest at both sides as shown in Fig. 6. The maximum motor torque on the magnetic rotor was 21.50 N-mm at 90 ° in-between stator and rotor electromagnetic forces. The torque per meter (m) produced in the permanent magnetic was origigth of 0.03 m is multiplied, then the total torque endsnally calculated as 717.0 N-m and if the len up with 21.50 N-mm. The minimum torque was 19.95 N-mm at 60 ° or 120 °. The torque per meter was originally calculated as 665.0 N-m at 60 ° and 120 °. As a result, the computed average torque of the maximum and minimum values is 20.725 N-mm. The average measured torque of a real DLDC motor is 20.46 N-mm at 28,000 rpm and 60 W of power output. The numerical analysis predicts the torque output accurately, compared with experiments.

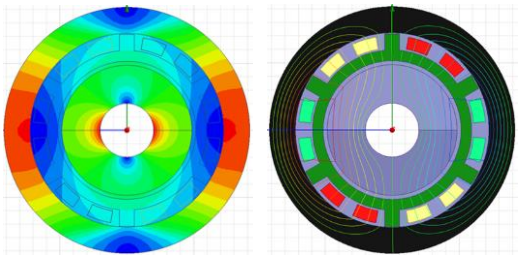

(a) Magnetic flux density and magnetic flux at 90 °

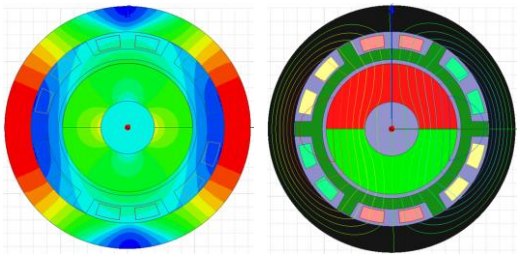

(b) Magnetic flux density and magnetic flux at 120 °

Figure 6. Distribution of magnetic flux density and magnetic flux in cases of 90 ° and 120 ° in-between two electromagnetic forces.

A parametric study was performed in an effort to improve the torque output by changing the number of coils and the shape and material of the stator. The torque outputs of the BLDC motor were calculated on the basis of the cross-sectional area of one coil as the number of coils increases. To add more coils, more space is required without an increase in motor diameter. The outer diameter of the motor and R_1 (=5.95 mm) in Fig. 7 are therefore fixed, and R_x can increase from 7.225 mm to R_{max} = 9.175 mm to secure more space for coils.

The area of a single coil cross-section is 0.513 mm^2, and one slot occupies 50 °. The two bunches of coils in an angle of 50 ° are placed as shown in Fig. 7. The number of coils can be related with the space parameter, R_x, as in (1).

$$0.153\text{mm}^2 \times \text{number of coils} = \pi\left(R_x^2 - R_1^2\right)\frac{50}{360}. \quad (1)$$

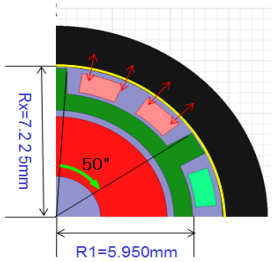

Figure 7. Dimensions of a quarter motor.

TABLE I: CHANGES IN COIL CROSS-SECTIONAL AREA AND RX WITH RESPECT TO THE NUMBER OF COILS AT 90 °

No.(coil wires)	Coil area (cross-section) (mm^2)	R_1 (mm)	R_x (mm)	R_{max} (mm)	A_{max} (mm^2)
12	3.665	5.950	7.225	9.175	10.642
13	3.970		7.321		
14	4.276		7.416		
15	4.581		7.510		
16	4.886		7.603		
17	5.192		7.694		
18	5.497		7.785		
19	5.803		7.874		
20	6.108		7.962		
21	6.413		8.050		
22	6.719		8.136		
23	7.024		8.222		
24	7.330		8.307		
25	7.635		8.390		
26	7.940		8.473		
27	8.246		8.556		
28	8.551		8.637		
29	8.857		8.718		
30	9.162		8.798		
31	9.467		8.877		
32	9.773		8.955		
33	10.078		9.033		
34	10.384		9.110		
35	10.689		9.187		

Fig. 7 shows quarter dimensions of a present BLDC motor used for a parametric study. There are 12 coil wires wound in one bunch of coils, and the required average cross-sectional area for a single wire is 0.153 mm^2. The maximum area for all wires is 10.642 mm, calculated

using (1). The motor torque was calculated as the number of coil wires changed at the angles of 60 ° or 90 ° between the electromagnetic field directions of the rotor and the stator. The coil area changes proportionally as the number of coil wires varies. The changes in coil cross-sectional area and R_x with respect to the number of coils at 90 ° are tabulated in Table I. Figs. 8(a), (c), and (e) show the cross-sectional models of the stator and rotor with 11, 20, and 30 coils, respectively. It is shown that the cross-sectional areas of the cover structure (i.e., the thickness of the outer circle) in the figure reduce as the internal coil areas increase. Figs. 8(b), (d), and (f) show the corresponding distribution of magnetic flux densities of the models in Figs. 8(a), (c), and (e), respectively.

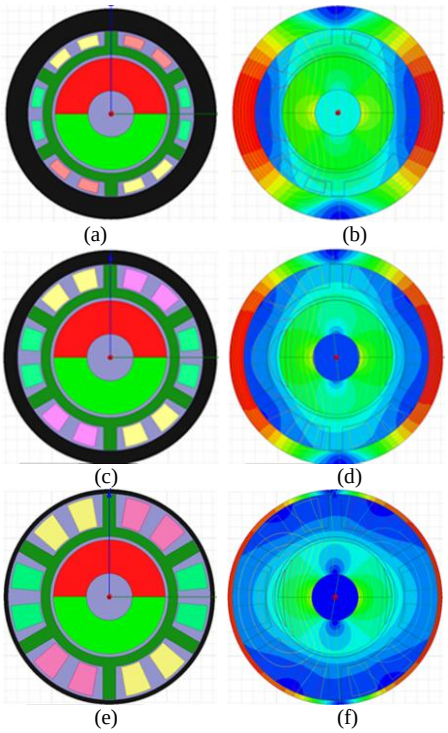

Figure 8. (a) A model of 15 coils, (b) magnetic flux density of a 15-coil model, (c) a model of 20 coils, (d) magnetic flux density of a 20-coil model, (e) a model of 30 coils, and (f) magnetic flux density of a 30-coil model, all at 90 °.

As the number of coil wires increases, the area also increases and the thickness of the motor cover decreases. Figs. 9 and 10 show the motor torque outputs per unit mm calculated using MAXWELL with different numbers of coil wires from 11 to 30 at 60 ° and 90 °. The maximum motor torque was obtained using 20 wound wires in both cases of electromagnetic angles as shown in Figs. 9 and 10. The trend in torque variations is that the torque increases as the wire number increases up to 20, and then, it decreases gradually even though the wire number increases. As expected, the torque at 90 ° is higher than that at 60 °.

In another study to increase the torque output, two different materials, Teflon and steel, for the stator slot were considered at an angle of 90 ° between the electromagnetic field directions of the stator and the rotor. Because that magnetic permeability of a Teflon slot is smaller than that of a steel slot, the magnetic flux density and the electromagnetic field of a BLDC motor may be changeable. Figs. 11(a) and (b) show the distribution of magnetic flux density with a steel slot and the magnetic lines of the flux with a steel slot at 90 °, respectively. It is shown in Fig. 11(b) that the large magnetic flux density is concentrated near a slot. The torque per meter produced by the steel slot was originally calculated as 543.0 N-m, and if the slot length of 0.03 m is multiplied, then the total torque becomes 16.29 N-mm, which is 79.6% of the Teflon slot torque. The result means that the Teflon slot is better than the steel one.

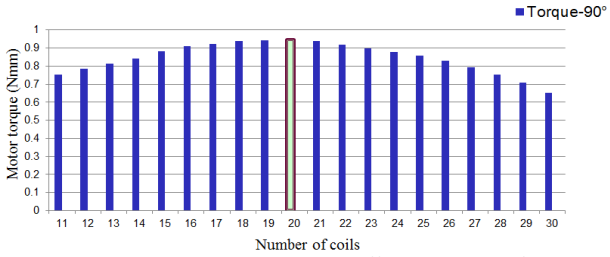

Figure 9. Motor torque per unit mm with different numbers of coil wires at 90 °.

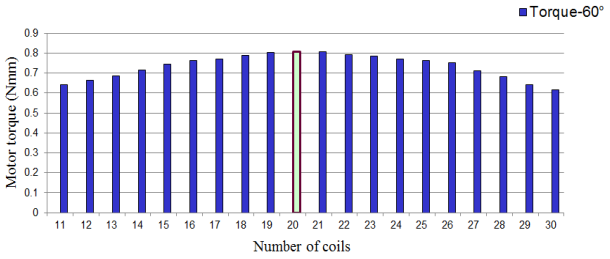

Figure 10. Motor torque per unit mm with different numbers of coil wires at 60 °.

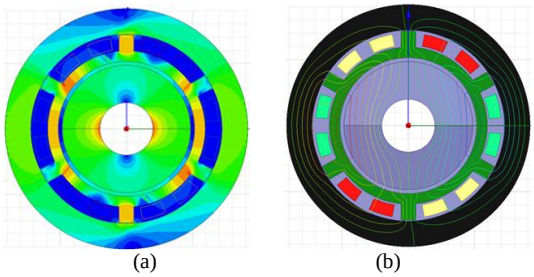

Figure 11. (a) Distribution of magnetic flux density with a steel slot and (b) magnetic lines of the flux with a steel slot at 90 °.

III. Ripple Analysis

A motor torque ripple is defined as a percentage of the difference between the maximum torque and the minimum torque compared to the average torque. It is caused by cogging torque and mechanical imbalances and occurs because of the variation in torque per one revolution. The torque ripple is evaluated based on the following equation [22]:

$$\text{Torque Ripple} = \frac{T_{\max} - T_{\min}}{(T_{\max} + T_{\min})/2} \times 100(\%), \quad (2)$$

where $T_{\max}$ and $T_{\min}$ denote the maximum and minimum torque values, respectively.

Torque ripple in electrical motors is generally undesirable, since it causes vibrations and noise, and might reduce the lifetime of the BLDC motor. Extensive

torque ripple requires measures such as skewing or changes to the motor geometry that might reduce the general performance of the BLDC motor. In addition to the cogging torque, the torque ripple can be caused by the interaction between the magneto-motive force (MMF) and the airgap flux harmonics. This MMF ripple can be influenced by variations in the geometry of the motor design; in particular, the number of stator slots, the number of poles, the magnet angle, and the slot opening width are important parameters to be investigated.

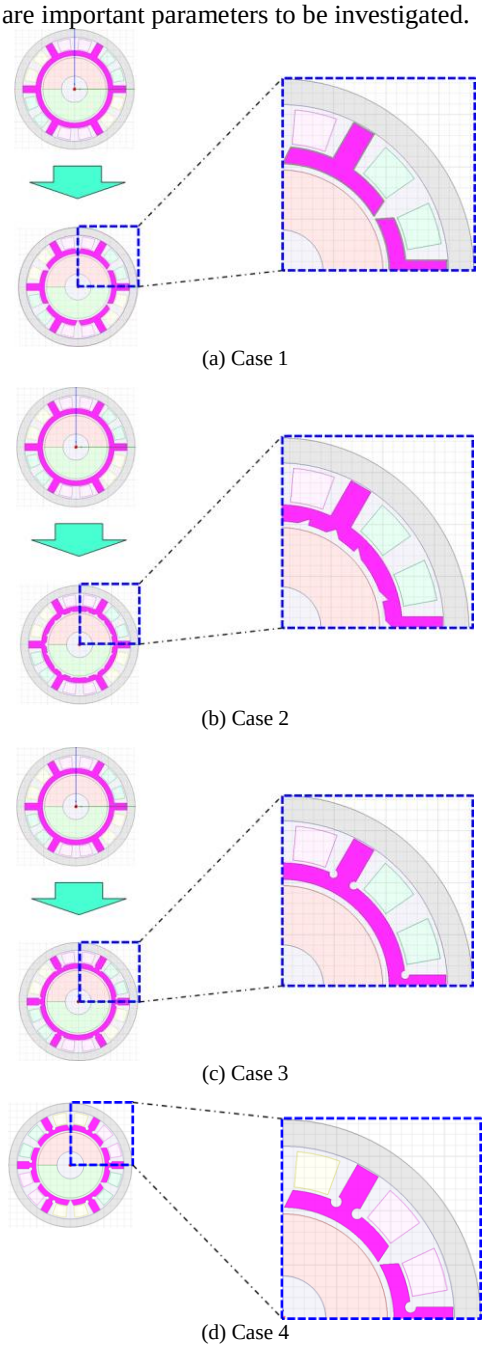

(a) Case 1

(b) Case 2

(c) Case 3

(d) Case 4

Figure 12. Four different cases of slot shapes in a state used for the computation of the torque ripple.

In an effort to reduce the torque ripple, four different cases of slot shapes in a stator were designed, and the torque ripples were compared. The computed torque ripple for the current slot with 20 coils is 7.8%. The four cases of design changes in a slot configuration are depicted in Fig. 12. The maximum and minimum torque values of the four cases are summarized in Table II. The torque ripples for cases 1, 2, 3, and 4 are calculated as 6.75%, 7.85%, 7.20%, and 6.10% on the basis of (2), respectively. The motor slot shape of case 4 gives least torque ripple among all four cases.

TABLE II. MAXIMUM AND MINIMUM TORQUE VALUES OF THE FOUR DIFFERENT CASES

Case	Maximum torque (90 °)	Minimum torque (60 °)
1	0.933 Nm	0.815 Nm
2	0.941 Nm	0.806 Nm
3	0.938 Nm	0.812 Nm
4	0.929 Nm	0.821 Nm

IV. CONCLUSIONS

Through electromagnetic modeling and analyses, methods in improving the torque output of a hand-piece BLDC motor have been studied. The average torque calculated from the existing reference motor was 20.73 N-mm, and the measured torque was 20.46 N-mm. The analysis method is accurate because the numerical results correlate with the measured ones. In an effort to improve the torque of the reference motor further, some case studies on the electromagnetic torque were performed using various numbers of wound coil wires from 11 to 30, and the maximum motor torque was obtained using 20 wound wires at an electromagnetic angle of 90 °. To reduce the torque ripple of the motor, the changes in torque ripples for several slot shapes in a stator were evaluated and compared. The slot with both circular holes and V-cuts showed the best ripple performance of 6.10%, compared to 7.80% of the current design.

ACKNOWLEDGMENT

This work was supported by the National Research Foundation of Korea (NRF) grant funded by the Korea government (MSIP) (2015R1A2A2A01007652).

REFERENCES

[1] J. E. Dyson and B. W. Darvel, "The development of the dental high speed air turbine handpiece-Part 1," *Australian Dental Journal*, vol. 38, no 1, pp. 49-58, 1993.
[2] J. E. Dyson and B. W. Darvel, "The development of the dental high speed air turbine handpiece-Part 2," *Australian Dental Journal*, vol. 38, no 29, pp. 131-143, 1993.
[3] S. H. Suh, Y. Choi, H. W. Roh, and H. Doh, "Flow analysis in the bifurcated duct with PIV system and computer simulation," *Trans. of the KSME(B)*, vol. 23, no. 1, pp. 123-180, 1999.
[4] C. Kim, J. Y. Kim, J. H. Lee, and S. H. Kwak, "Strength analyses of new 2- and 3- axis-type small multiplying gears in dental hand-piece," *Trans. of KSME A.*, vol. 36, no. 9, pp. 1027-1032, 2012.
[5] J. E. Dyson and B. W. Darvel, "Flow and free running speed characterization of dental air turbine hand-piece," *Journal of Dentistry*, vol. 27, pp. 456-477, 1999.
[6] M. C. Han, "Development of ultra-high speed dental hand-piece," *Trans. of the KSME*, pp. 68-72, 2008.
[7] H. H. Kim, T. J. Je, J. C. Jeon, H. J. Choi, C. E. Kim, K. M. Lee, B. W. Kong, and T. M. Kim, "Study on precision balancing method of BLDC motor shaft for the application of medical hand-piece," in *Proc. the KSMPE Spring Conf.*, Korea, 2013, p. 133.

[8] J. E. Dyson and B. W. Darvel, "Torque, power and efficiency characterization of dental air turbine hand-piece," *Journal of Dentistry*, vol. 27, pp. 573-586, 1999.
[9] T. W. Kong, S. H. Park, J. S. Yu, B. K. Lee, and C. Y. Won, "Drive system of battery type surgical hand-piece," in *Proc. Korean Inst. Illuminating and Elect. Install. Engineers*, 2007, pp. 64-66.
[10] E. H. E. Bayoumi and Z. A. Salmeen, "Practical swarm intelligent control brushless DC motor drive system using GSM technology," *WSEAS Trans. on Circuits and Systems*, vol. 13, pp. 188-201, 2014.
[11] A. H. O. Ahmed, "High performance speed control of direct current motors using adaptive inverse control," *WSEAS Trans. on Systems and Control*, vol. 7, pp. 54-63, 2012.
[12] R. A. Habibabadi and A. Nekoubin, "Analysis and simulation of single-phase and two-phase axial flux brushless DC motor," *WSEAS Trans. on Power Systems*, vol. 8, pp. 1-11, 2013.
[13] J. Yoo, N. Kikuchi, and J. L. Volakis, "Structural optimization in magnetic devices by the homogenization design method," *IEEE Trans. on Magnetics*, vol. 36, no. 3, pp. 574-580, 2000.
[14] J. Yoo, N. Kikuchi, and J. L. Volakis, "Structural optimization in magnetic fields using the homogenization design method-Part I," *Archives of Computational Methods in Engineering State of the Art Reviews*, vol. 8, no. 4, pp. 387-406, 2001.
[15] J. Yoo, N. Kikuchi, and J. L. Volakis, "Structural optimization in magnetic fields using the homogenization design method-Part II," *Archives of Computational Methods in Engineering State of the Art Reviews*, vol. 9, no. 3, pp. 257-282, 2002.
[16] H. Moradi, E. Afhei, and F. Faghihi, "FEM Analysis for a novel configuration of brushless DC motor without permanent magnet," *Progress in Electromagnetics Research, PIRE98*, pp. 407-423, 2009.
[17] C. L. Chiu, Y. T. Chen, Y. L. Liang, and R. H. Liang, "Optimal driving efficiency design for the single-phase brushless DC fan motor," *Progress in Electromagnetics Research*, *PIRE98*, pp. 407-423, 2010.
[18] M. Sanada, K. Hiramoto, S. Morimoto, and Y. Takeda, "Torque ripple improvement for synchronous reluctance motor using an asymmetric flux barrier arrangement," *IEEE Trans. Ind. Appl*., vol. 40, no. 4, pp. 1076-1082, 2004.
[19] S. I. Kim, J. Y. Lee, Y. K. Kim, J. P. Hong, Y. Hur, and Y. H. Jung, "Optimization for reduction of torque ripple in interior permanent magnet motor by using the Taguchi method," *IEEE Trans. on Magnetics*, vol. 41, no. 5, pp. 1796-1799, 2005.
[20] K. Kioumarsi, M. Moallem, and B. Fahimi, "Mitigation of torque ripple in interior permanent magnet motor by optimal shape design," *IEEE Trans. on Magnetics*, vol. 42, no. 11, pp. 3706-3711, 2006.
[21] J. Kwack, S. Min, and J. P. Hong, "Optimal stator design of interior permanent magnet motor to reduce torque ripple using the level set method," *IEEE Trans. on Magnetics*, vol. 46, no. 6, pp. 2108-2111, 2010.
[22] S. Lim, S. Min, and J. P. Hong, "Low torque ripple rotor design of the interior permanent magnet motor using the multi-phase level-set and phase-field concept," *IEEE Trans. on Magnetics*, vol. 48, no. 2, pp. 907-910, 2012.
[23] M. R. Babu, P. S. V. Kishore, and Y. R. Sankar, "Commutation torque ripple minimization in brushless DC motor by genetic algorithm (GA) based PI-controller," *Journal of Control and Systems Engineering*, vol. 4, no. 1, pp. 20-31, 2016.
[24] X. Liu, Z. Gu, and J. Zhao, "Torque ripple reduction of a novel modular arc-linear flux-switching permanent-magnet motor with rotor step skewing," *Energies*, vol. 9, pp. 404-421, 2016.
[25] Y. Ozoglu, "New magnet shape for reducing torque ripple in an outer-rotor permanent-magnet machine," *Turkish Journal of Electrical Engineering & Computer Sciences*, vol. 25, pp. 4381-4397, 2017.
[26] B. Tan, Z. Hua, L, Zhang, and C. Fang, "A new approach of minimizing commutation torque ripple for BLDCM," *Energies*, vol. 10, pp. 1735-1748, 2017.

Cheol Kim was born in Korea and received Ph.D. degree in January, 1995 from University of Illinois at Urbana-Champaign, USA. His major field of study is mechanics of anisotropic materials and design optimization.

Mingzhe Li was born in China and received his master degree in the mechanical engineering from Kyungppok National University, Daegu, Korea.